

The Research on Corrosion Properties of Some Magnesium Alloys for Biomaterials

Ya Zhang^{1,2}, Sen Wu¹, Qiurong Chen^{1,2}, Xuehua Zhou^{1,2}, Zhongling Wei¹

¹ Shanghai Institute of Microsystem and Information Technology, Chinese Academy of Sciences, 865 Changning Road, Shanghai, P.R.China(200050)

² Jiaxing Light Alloy Engineering Technology Center, Chinese Academy of Sciences
778 Yatai Road, Jiaxing, P.R.China(314022)

*E-mail: yzhang@mail.sim.ac.cn

Received: 26 May 2014 / Accepted: 25 September 2014 / Published: 2 December 2014

Metals which consist of elements existing in the human body are promising candidates for planting materials. Many magnesium alloys are developed as degradable implanting alloys with improved mechanical properties and enhanced corrosion properties. In this paper, the corrosion properties of these tested alloys are studied for biomaterial through the immersion test and electrochemical potentiodynamic polarization test. The microstructure before and after immersion tests was observed by optical Microscopy and fieldemission scanning electron Microscope. The mechanical properties of these alloys were studied by Universal Testing Machine. The influence of different elements in magnesium alloys on the corrosion properties was analyzed in this paper.

Keywords: degradable planting alloy, magnesium alloys, corrosion properties, mechanical properties;

1. INTRODUCTION

Metals which consist of elements existing in the human body are promising candidates for planting materials. Magnesium alloy have received more and more attentions as degradable biomaterial.

Magnesium alloy is lightest material among structural material. The elastic modules and compressive yield strength of magnesium alloy is closer to natural bone than other metallic implants[1]. Many commercial magnesium alloys were adopted to study as biomaterial, such as WE43, AZ31, AZ91, AM60B etc[2-26]. At the early stage of research, the strength, creep strength and thermal stability are the main concerns[27-29]. In recent years, it was found that the magnesium biomaterial was disadvantaged as the high corrosion rates and undesirable biocompatibility problem[13]. The corrosion rate was main concern in a lot of research because they are closely related

to degradation rates and biocompatibility[14,16]. The rapid corrosion of magnesium is the key obstacle for the clinical use of magnesium alloys, which needs to be addressed before surgical implantation. Many magnesium alloys are developed as implanting alloys with improved mechanical properties and enhanced corrosion properties.

In this paper, the corrosion properties of material are studied for biomaterial. The corrosion properties are determined by the elements and impurities of magnesium. The influence of different elements in magnesium alloys on the corrosion properties were analyzed in this paper.

2. EXPERIMENTALS

Table 1. Chemical composition of the studied alloys

	Al	Zn	Mn	Ce	La	Nd	Y	Si	Cu	Ni	Fe	Mg
WE43					0.09	2.65	3.73	0.013	0.0020	<0.0015	<0.0012	Bal.
AZ31	2.98	1.16	0.209					0.015	0.0023	<0.0015	<0.0012	Bal.
AZ31+RE	2.87	1.17	0.213	0.233	0.080	0.069		0.020	0.0018	<0.0015	<0.0012	Bal.
AZ31+LaPrCe	3.10	1.15	0.229	0.075	0.267	0.022		0.017	0.0015	<0.0015	<0.0012	Bal.
AZ11	1.09	1.11	0.180					0.023	0.0020	<0.0015	<0.0012	Bal.
AZ11+RE	1.11	1.15	0.180	0.261	0.089	0.067		0.018	0.0019	<0.0015	<0.0012	Bal.
AZ11+LaPrCe	1.08	1.15	0.229	0.083	0.256	0.027		0.015	0.0015	<0.0015	<0.0012	Bal.

Chemical compositions of the studied alloys are listed in Table 1. These alloys were melted in a mild steel crucible with the protection of a mixed gas atmosphere of SF₆ (1 vol.%) and CO₂ (99%). The ingots were homogenized at 400°C for 18 h and then hot-extruded into rods with diameter of 2 mm at 350°C with the extrusion ratio 38:1. The specimens used for the tests were in the form of dimensions 14×14×4 mm machined in the extruded alloys.

These alloys were tested in artificial plasma (NaCl: 6.800g/L CaCl₂ 0.200g/L KCl: 0.400g/L MgSO₄: 0.100g/L NaHCO₃: 2.200g/L Na₂HPO₄: 0.126g/L NaH₂PO₄: 0.026g/L). The corrosion rates of different Mg alloys were measured and compared by the immersion corrosion tests in artificial plasma at 37°C for 2, 7 and 30 days. After the immersion tests, the samples were exposed to chromic acid solution for about 10 minutes to remove the corrosion products of sample surface and then the samples were washed by deionization water, dried and weighted. The corrosion rates of different Mg alloys were measured by determining the weight loss of different samples.

The electrochemical potentiodynamic polarization curves of the alloys are measured in artificial plasma at 37°C, using Autolab 302N. The microstructure of these extruded alloys was studied by Leical optical Microscopy. The surface and section of these alloys after the immersion tests was studied by Hitachi fieldemission scanning electron microscope.

3. RESULTS AND DISCUSSION

3.1 The corrosion properties of studied alloys

The immersion corrosion tests are the simplest of the in vitro methods for investigating the corrosion of Mg, which has led to their relative popularity.

Results obtained from the tests are typically accurate, assuming that issues with the removal of the corrosion layer are minimized.

The corrosion rates of different Mg alloys were measured and compared by the immersion corrosion tests in artificial plasma at 37°C for 2 and 30 days. Fig.1 shows the corrosion rate of these as-extruded alloys in artificial plasma for two days. It can be concluded that the corrosion rate of WE43 alloy (about 0.6 mm/y) is more than any other alloys. From the biggest to the smallest of corrosion rates, the sequence of these alloys are WE43, AZ11, AZ11+LaPrCe, AZ11+RE and AZ31+LaPrCe. The corrosion rate of AZ31+LaPrCe alloy (0.172 mm/y) is smallest among these alloys.

As shown in Fig.1 and Fig.2, the corrosion rate of AZ11+RE alloy increase steadily with the testing time, which can control the rapid corrosion rate of the magnesium alloys to some extent. The corrosion rates of AZ31 and so on increase rapidly, which can make these planting alloys lose their strength too early. Aluminium elements can cause muscle fiber damage [30], and decrease osteoclast viability[31,32]. As a result, the low aluminium elements can reduce the risk of the awful biocompatibility which the high aluminium elements cause in magnesium alloys. As a result, AZ11+RE alloy is more appropriate implant materials than other alloys.

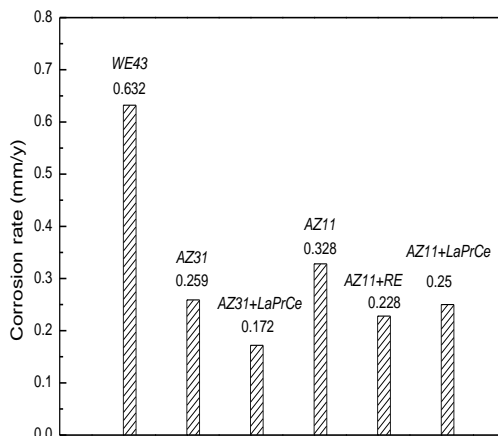


Figure 1. The corrosion rates of these as-extruded alloys in artificial plasma for two days at 37°C

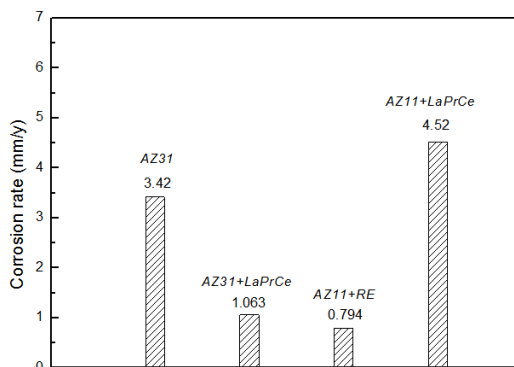


Figure 2. The corrosion rate of these as-extruded alloys in artificial plasma for 30 days at 37°C

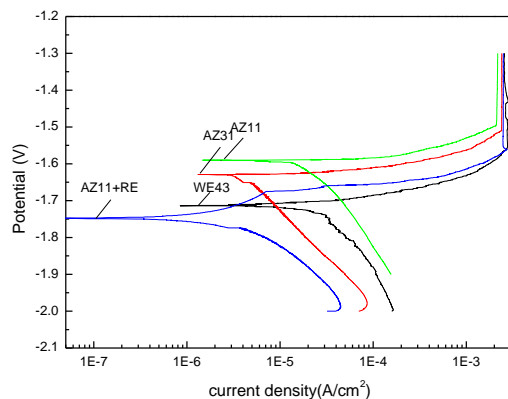


Figure 3. The potentiodynamic polarization curves of these alloys in artificial plasma

As shown in Fig.2, the corrosion rates of AZ31 alloy and AZ11+LaPrCe alloy for 30 days increase greatly, compared with the corrosion rates for 2 days. However, the corrosion rates of AZ31+LaPrCe alloy and AZ11+RE alloy for 30 days increase less greatly than AZ31 alloy and AZ11+LaPrCe alloys, compared with the corrosion rates for 2 days. The corrosion rates of AZ11+RE alloy is smallest among these alloys. It can be indicated that the corrosion rate of AZ11+RE alloy change steadily with the increase of testing time, which can meet the demand of controlling the rapid corrosion rates of the magnesium alloys to some extent.

Table 2. The corrosion potentials and corrosion currents of the alloys

Alloy code	Nominal composition	E_{corr} (V) (SCE)	I_{corr} ($\mu A/m^2$)
T1	WE43	-1.71	27.7
T2	AZ31	-1.62	4.3
T3	AZ11	-1.59	23.2
T4	AZ11+0.5RE	-1.75	3.2

Fig.3 shows that the potentiodynamic polarization curves of WE43, AZ31, AZ11 and AZ11+RE alloys. Table 2 shows the corrosion currents and corrosion potentials of these alloys. With the addition of RE in AZ11 alloy, the corrosion potential decreased. It can also be shown that the corrosion current of AZ11+RE alloy is smallest among these alloys, which shows that the alloy has the best corrosion resistance among these alloys. The corrosion current of AZ11 and WE43 alloy are larger than other alloys, which shows that the alloys have the less corrosion resistance among these alloys. The potentiodynamic polarization anodic curve of AZ11+RE alloy shows apparent turning point, which indicates the pitting potential. The corrosion of Mg will result in Mg^{2+} and reduce H_2O , releasing H_2 gas and hydroxyl ($(OH)^{-1}$) ions into the corrosion medium. Additionally, the corrosion rate of Mg monotonically decreases as a function of increasing pH with passivation attained at a PH 12 [33]. The passivation took place between the corrosion potential and the pitting potential. As shown in Fig 3, there was no obvious passivity among other alloys. It can be concluded that the results of the

potentiodynamic polarization curves almost coincide with the results of immersion corrosion tests, which shows that the corrosion resistance of AZ11+RE alloy are better than other alloys.

3.2 The microstructure analysis before immersion tests and after immersion tests

Fig. 4-9 show the optical microstructure photograph of as-extruded WE43, AZ31, AZ31+LaPrCe, AZ11, AZ11+RE and AZ11+LaPrC alloys. From these figures, it can be shown that dynamic recrystallization process had finished completely in these alloys during the extrusion. Moreover, the sizes of dynamic recrystallization grains in these alloys are different. As shown in Fig. 4, the secondary phases were fine and dispersive, which leads to the formation of fine and uniform recrystallization grains. The large amount of aluminum element in AZ31 and AZ31+LaPrCe alloys results in the formation of more amount of the secondary phase $Mg_{17}Al_{12}$, which leads to the formation of fine and uniform recrystallization grains, as shown in Fig.5 and Fig.6.

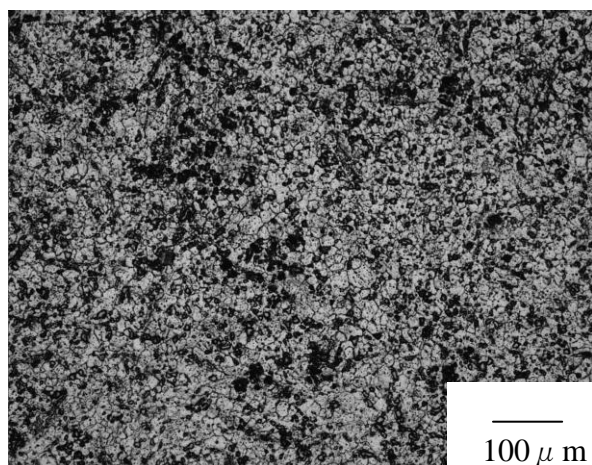


Figure 4. The optical microstructure photograph of as-extruded WE43 alloy.

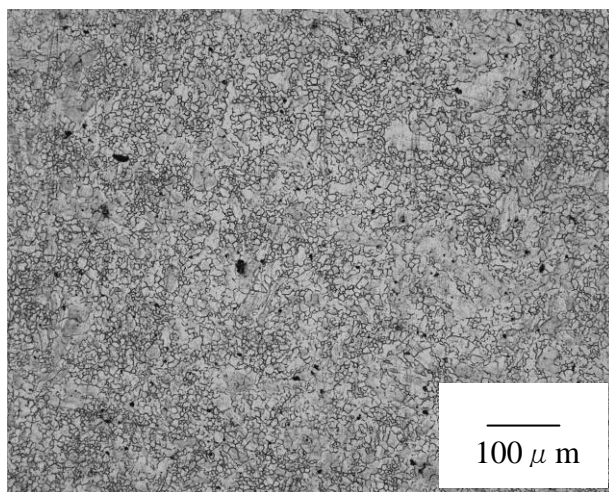


Figure 5. The optical microstructure photograph of as-extruded AZ31 alloy.

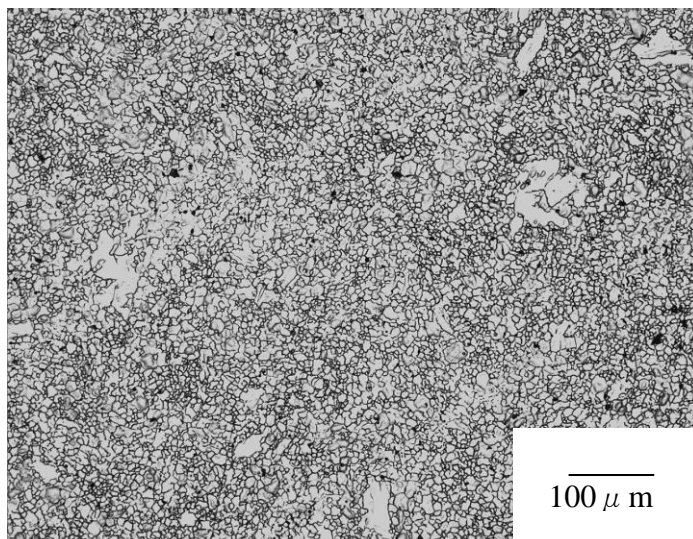


Figure 6. The optical microstructure photograph of as-extruded AZ31+LaPrCe alloy.

The small amount of aluminum element in AZ11, AZ11+RE and AZ11+LaPrC alloys results in the formation of less amount of the secondary phase Mg₁₇A₁₂, which leads to the formation of large and nonuniform recrystallization grains, as shown in Fig.7 and Fig.8. Compared between Fig. 7 and Fig. 8, the recrystallization grains in AZ11+RE alloy are finer and more uniform than these in AZ11 alloy. It is due to that the addition of RE can prevent recrystallization grains from growing.

Fig.10 shows the photography of the surface and section of WE43 alloy in artificial plasma for 15 days at 37°C, which shows the thick corrosion film covered on the surface of WE43 alloy in artificial plasma for 15 days.

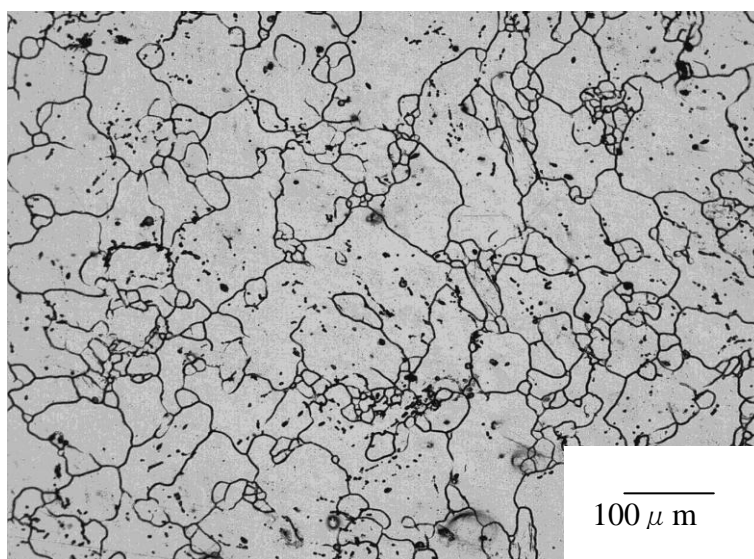


Figure 7. The optical microstructure photograph of as-extruded AZ11 alloy.

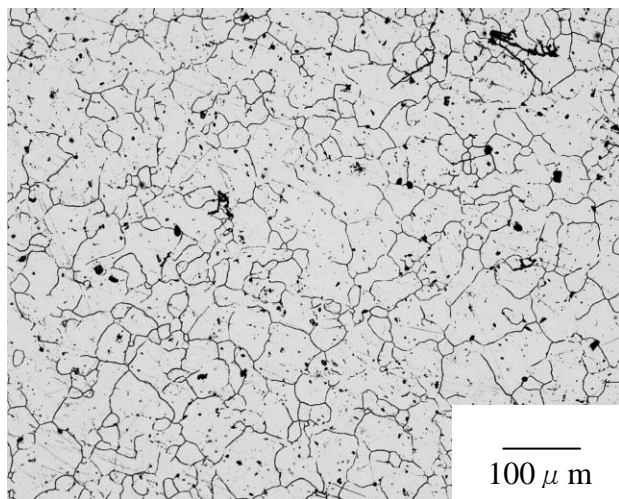


Figure 8. The optical microstructure photograph of as-extruded AZ11+RE alloys

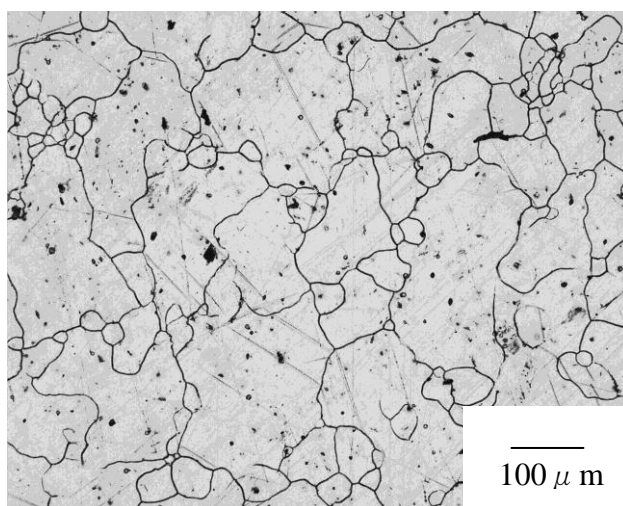


Figure 9. The optical microstructure photograph of as-extruded AZ11+LaPrCe alloy.

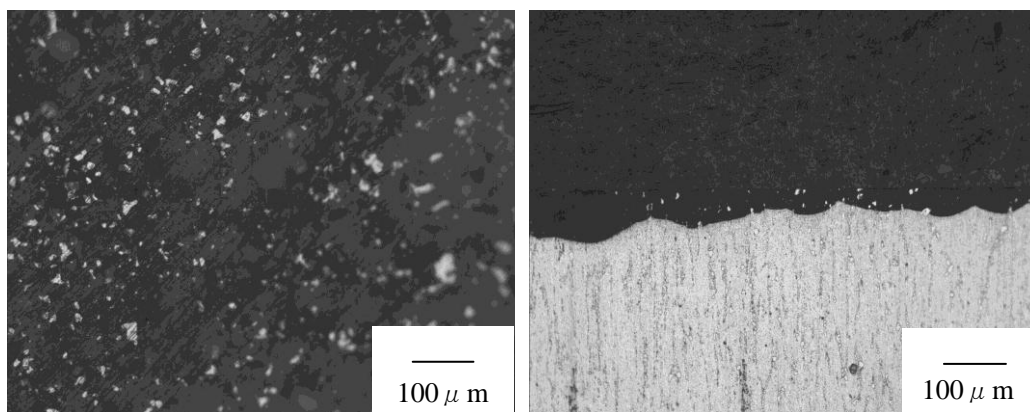


Figure 10. The photography of the surface and section of WE43 alloy in artificial plasma for 15 days at 37°C

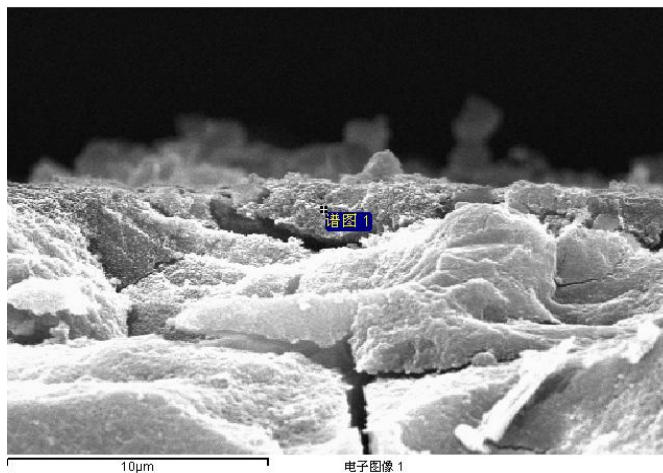


Figure 11. The SEM photograph of the section of WE43 alloy in artificial plasma for 15 days at 37°C

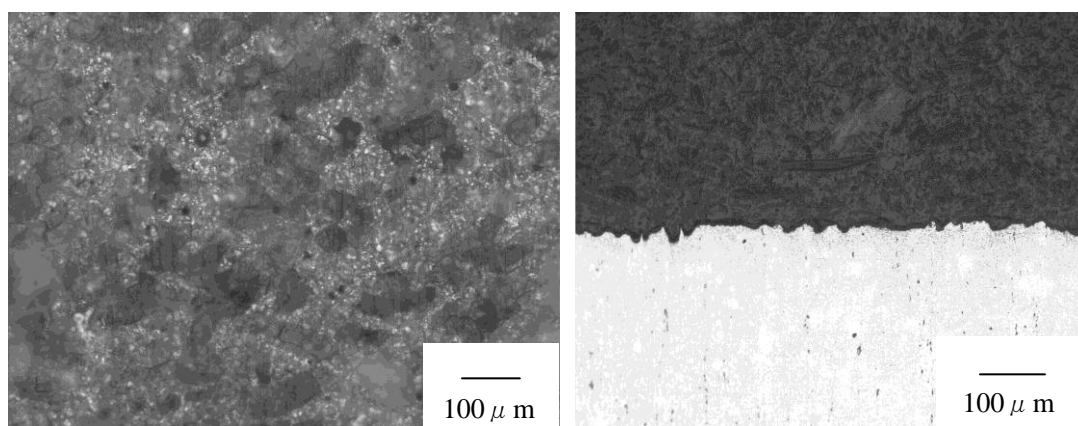


Figure 12. The photography of the surface and section of AZ11+RE alloy in artificial plasma for 15 days at 37°C

Table 3. The EDS analysis of the point located in Fig.11

elements	Weight percent(%)	Elements percent(%)
O	65.51	75.72
Mg	26.73	20.34
P	2.20	1.31
Cl	1.13	0.59
K	0.07	0.03
Ca	4.37	2.02

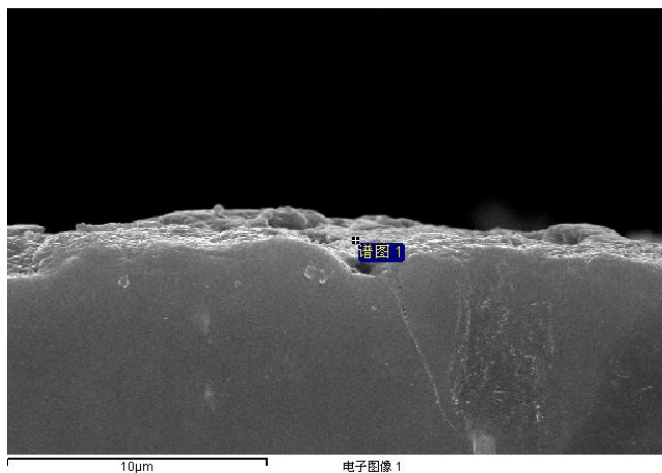


Figure 13. The photography of the section of AZ11+RE alloy in artificial plasma for 15 days at 37°C

Table 4. The EDS analysis of the point located in Fig.13

elements	Weight percent(%)	Elements percent(%)
O	12.43	17.73
Na	1.19	1.19
Mg	86.37	81.08

Fig.11 show the section of WE43 alloy in artificial plasma for 15 days at 37°C, and Table 3 shows the EDS analysis of the point located in Fig.11. It can be concluded that the thick oxide layer is mainly composed of magnesium and oxygen elements with small amount of phosphorus, chloride, potassium and calcium elements. Because of severe corrosion attack in the alloy, the phosphorus, chloride, potassium and calcium elements from artificial plasma enter the matrix of the alloy. As shown in Tab. 3, the element percent of oxygen is up to 75.7%.

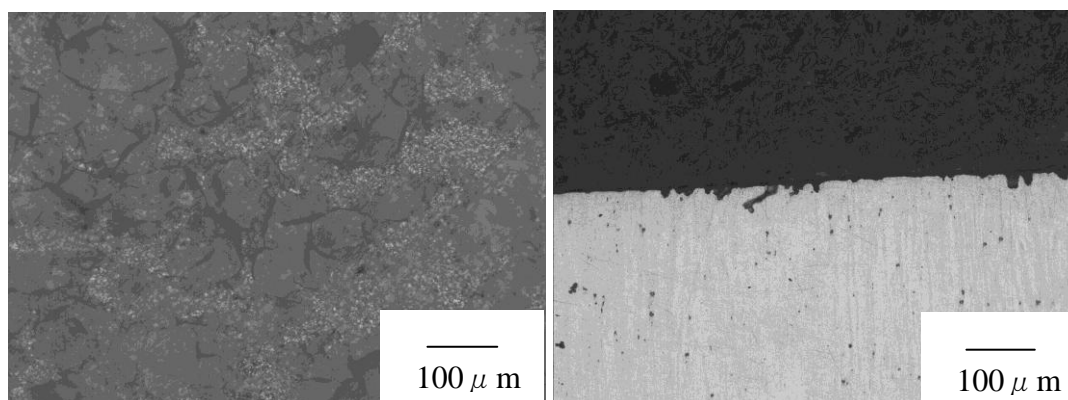


Figure14. The photography of the surface and section of AZ31 alloy in artificial plasma for 15 days at 37°C

Fig. 12 shows the photography of the surface and section of AZ11+RE alloy in artificial plasma for 15 days at 37°C. Compared with WE43 alloy, the corrosion layer of AZ11+RE alloy partly covers the surface of the alloy, which does not penetrate into the matrix of the alloy.

Fig.13 show the section of AZ11+RE alloy in artificial plasma for 15 days at 37°C, and Table 4 shows the EDS analysis of the point located in Fig.13. It can be concluded that the thin oxide layer consists of magnesium and oxygen elements without phosphorus, chloride, potassium and calcium elements from artificial plasma. Because of mild corrosion attack in the alloy, the phosphorus, chloride, potassium and calcium elements from artificial plasma do not enter the matrix of the alloy.

From the microstructure and EDX analysis of AZ11+ RE alloy in Fig.13 and Table 4, the corrosion could not penetrate the alloy and only cause mild damage in the alloy. As shown in Tab. 4, the element percent of oxygen is up to 17.7%

Fig. 14 shows the photography of the surface and section of AZ31 alloy in artificial plasma for 15 days at 37°C. Compared with AZ11+RE alloy, the corrosion layer of AZ31 alloy is thicker.

Fig.15 show the section of AZ31 alloy in artificial plasma for 15 days at 37°C, and Table 5 shows the EDS analysis of the point located in Fig.15. It can be concluded that the oxide layer is mainly composed of magnesium and oxygen elements with small amount of chloride element from artificial plasma. It is due to that the local corrosion could penetrate into the alloy to a small extent and so chloride element enter the matrix of the alloy. As shown in Tab. 5, the element percent of oxygen is up to 21.9%.

Among these alloys, the element percent of oxygen in AZ11+RE alloy is lowest and so the corrosion cause most mild damage in this alloy. It may be ascribed to that the addition of RE in magnesium alloy can lead to the formation of Mg-RE phase, which can prevent the corrosion from developing.

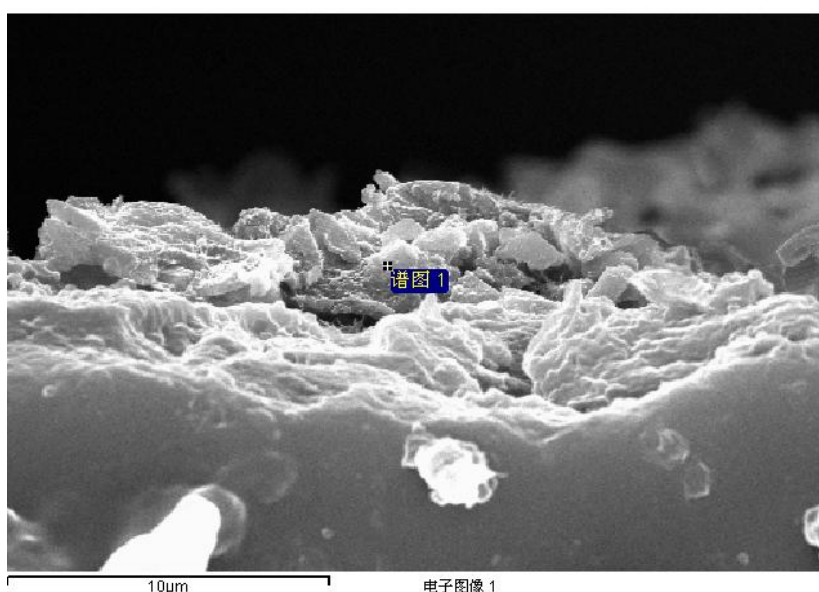


Figure 15. The photography of the section of AZ31 alloy in artificial plasma for 15 days at 37°C

Table 5. The EDS analysis of the point located in Fig.15

elements	Weight percent(%)	Elements percent(%)
O	15.58	21.91
Mg	84.30	78.01
Cl	0.11	0.07

3.3 The mechanical properties of studied alloys

Many magnesium alloys has been developed to improve the mechanical properties, which is required as implanting alloys.

Table 6. The mechanical properties of these alloys

specimen	tensile strength σ_b /MPa	yield strength $\sigma_{0.2}$ /MPa	elongation δ /%
WE43	280.5	205.6	9.2
AZ11	231.7	160.5	13.5
AZ31	250	175.8	14
AZ11+RE	283.5	217.3	11.8
AZ31+LaPrCe	307	209.5	14.1

As shown in Table 6, the tensile strength and yield strength of AZ11+RE, WE43 and AZ31+LaPrCe alloys are higher than other alloys. However, according to mechanical properties, the sequence of these alloys from the biggest to lowest are AZ31+LaPrCe, AZ11+RE, WE43, AZ31 and AZ11 respectively. The tensile strength of AZ11+ RE alloy reaches to 280MPa, which is high strength for magnesium alloy whose weight percent of total added elements is less than 2.5%. The mechanical properties of the alloy can meet the demand of mechanical properties of planting materials in the process of manufacturing and using.

4. CONCLUSIONS

(1) The corrosion rate of AZ11+RE alloy is smallest among these alloys in artificial plasma for 30 days. The corrosion rate of AZ11+RE alloy increase steadily with the testing time.

(2) The local corrosion could not penetrate into the matrix of AZ11+RE alloy and only cause mild damage in the alloy.

(3) The tensile strength of AZ11+ RE alloy reaches to 280MPa, whose mechanical properties of the alloy can meet the demand of mechanical properties of planting materials in the process of manufacturing and using.

ACKNOWLEDGEMENT

At the point of finishing this paper, I'd like to express my sincere thanks to all those who have lent me hands in the course of my writing this paper. This paper is funded by Shanghai Scientific Research Projects (11DJ1400302).

References

1. E. Wintermantel, S-W Ha. *Medizintechnik mit biokompatiblen Werkstoffen und Verfahren. 3rd ed.* Berlin, Heidelberg, New York: Springer; 2002.
2. L. P. Xu, G. N. Yu, E. Zhang, F. Pan, K. Yang, J. Biomed Mater Res A, 83(2007)703.
3. F. Witte, V. Kaese, H. Haferkamp, E. Switzer, A. Meyer-Lindenberg, C.J. Wirth, et al., *Biomaterials*, 26(2005)3557.
4. F. Witte, J. Fischer, J. Nellesen, H-A Crostack, V. Kaese, A. Pisch, *Biomaterials*, 27(2006)1013
5. GL. Song, A. Atrens, *Adv Eng Mater*, 1(1999)11.
6. F. Witte, H. Ulrich, M. Rudert, E. Willbold, *J Biomed Mater Res A*, 81(2007)748.
7. F. Witte, *Acta Biomater*, 6(2010)1680.
8. Z. Shi, A. Atrens, *Corros Sci*, 53(2011)226.
9. GD. Zhang, JJ. Huang, K. Yang, BC. Zhang, HJ. Ai, *Acta Metall Sin*, 43(2007)1186.
10. F. Witte, H. Ulrich, C. Palm, E. Willbold, *J Biomed Mater Res A*, 81(2007)757.
11. F. Witte, J. Reifenrath, PP. Muller, HA. Crostack, J. Nellesen, FW. Bach, *Materialwiss Werkstofftech*, 37(2006)504.
12. YB. Ren, JJ. Huang, K. Yang, BC. Zhang, Z Yao, H. Wang, *Acta Metall Sin*, 41(2005)1228.
13. WD. Müller, M. Zeddies, M. Córscico, *J Mater Res*, 10(2007)5.
14. N.T. Kirkland, N. Birbilis, M.P. Staiger, *Acta Biomaterialia*, 8(2012) 925.
15. H. Kuwahara, Y. Al-Abdullat, N. Mazaki, S. Tsutsumi, *Mater. Trans.*, 42(2001)1317.
16. MB. Kannan, RKS. Raman, *Biomaterials*, 29(2008)2306.
17. R. Rettig, S. Virtanen, *J. Biomed. Mater. Res. A*, 85(2008)167.
18. G.L. Song, S. Z. Song, *Adv. Eng. Mater.* 9(2007)298.
19. YW. Song, DY. Shan, EH. Han, *Mater. Lett.* 62(2008) 3276.
20. H. Wang, R. Akid, M. Gobara, *Corros. Sci.*, 52(2010)255.
21. H. Wang, Y. Estrin, Z. Zuberova, *Mater. Lett.*, 62(2008)2476.
22. QD. Wang, WD. Chen, XQ. Zeng, YZ. Lu, WJ. Ding, YP. Zhu, *J. Mater. Sci.*, 36(2001)3035.
23. F. Witte, F. Feyerabend, P. Maier, J. Fischer, M. Stormer, C. Blawert, *Biomaterials*, 28(2007)2163.
24. LP. Xu, EL. Zhang, DS. Yin, SY. Zeng, K. Yang, *J. Mater. Sci. Mater. Med.*, 19(2008)1017.
25. N. Von der Hoeh, A. Krause, CH. Hackenbroich, D. Bormann, A. Lucas, A. Meyer-Lindenberg, *Dtsch Tierarztl Wochenschr*, 113(2006)439.
26. CL. Liu, YC. Xin, XB. Tian, PK. Chu, *J. Mater. Res.*, 22(2007)1806.
27. HE. Friedrich, BL. Mordike, *Berlin, Heidelberg: Springer-Verlag*, 2006.
28. MM. Avedesian, *Materials Park, OH: ASM International*, 1999.
29. MEL., *Magnesium Elektron Datasheet 467: Elektron WE43*, 2005
30. M. Shingde, J. Hughes, R. Boadle, EJ. Wills, R. Pamphlett, *Med. J. Aust.*, 183(2005)145.
31. AV. Rousselle, D. Heymann, V. Demais, C. Charrier, N. Passuti, MF. Basle, *Histol Histopathol*, 17(2002)1025.
32. Sarah E. Henderson, Konstantinos Verdelis, *Acta Biomaterialia*, 10 (2014) 2323.
33. R. Winston, R. Herbert, H. Uhlig, *Corrosion and corrosion control. New York: Wiley*, (2008)43.